Imaging Neurologic Manifestations of Oncologic Disease

2

Raymond Huang and Patrick Y. Wen

Intracranial Metastasis

Brain metastases are the most common cause of malignant brain tumors in adults. Lung and breast cancers are the most common tumors that metastasize to brain, with melanoma, renal, and colorectal cancers accounting for the majority of the remaining metastases [1]. Among human cancers, melanoma has the highest propensity to metastasize to the brain [2]. The relative anatomical distribution of metastases in brain is associated with regional blood perfusion, with 80% of metastases found in supratentorial compartment, 15% in the cerebellum, and 5% in brainstem [3]. Metastatic tumors can involve either intra-axial or extra-axial compartments, or both.

Radiological Features of Intra-Axial Metastases

When metastases occur in brain parenchyma (intra-axial), the junction of gray and white matters is the most common site of seeding. Intra-axial metastatic lesions can be solid-appearing or demonstrate intratumoral necrosis or cystic changes as rimenhancement on contrast enhancement CT or MRI.

Unless intratumoral hemorrhage is present, metastases are usually isodense on unenhanced CT and often not readily distinguished from adjacent brain tissues. The presence of vasogenic edema characterized by hypodensities outlining the gray and white matter junction can be an important clue suggesting an underlying metastasis. For larger lesions with cystic or necrotic changes, the lesions appear hypodense compared to normal brain tissues. In a few subtypes of metastatic tumors including germ cell tumors, melanoma, small cell lung cancers, and lymphoma, the tumors cells are highly cellular resulting in increased attenuation on CT. Due to streak and beam hardening artifacts from dense osseous structures in the skullbase, small or isodense posterior fossa lesions can be difficult to detect on CT. Most metastases enhance intensely with iodinated contrast due to absence of blood–brain barrier within tumor vasculature. Contrast-enhanced CT remains a very commonly employed screening test for some tumor types since CT imaging of other body areas can be performed on the same day of brain CT and its cost is lower than that of MRI.

The cellular component of brain metastases on MRI is usually hypointense to isointense relative to gray matter on T1-weighted images and hypointense on T2-weighted images. The necrotic or cystic tumor components generally appear hypointense on T1-weighted images and hyperintense on T2-weighted images. A subset of metastases can exhibit hyperintensity on T1-weighted images due to presence of subacute blood product. The wall of the enhancing rim is usually thick and irregular, and this can be an important sign to differentiate from the usual thin rim of enhancement seen with brain abscesses.

More than half of brain metastases are multifocal, but a significant number will present as a solitary brain mass, making differentiation from primary brain tumors difficult [4]. The enhancing portions of tumor often have distinct sharp margins from adjacent brain parenchyma, in contrast to high-grade primary gliomas that typically exhibit an infiltrative pattern at the tumor–brain interface. In the following sections individual imaging features pertinent to the diagnosis of metastasis will be discussed (Table 2.1).

R. Huang (✉)
Department of Radiology, Brigham and Women's Hospital, 75 Francis Street, Boston, MA 02115, USA
e-mail: ryhuang@partners.org

P.Y. Wen
Center for Neuro-Oncology, Dana-Farber/Brigham and Women's Cancer Center, 450 Brookline Avenue, Boston, MA 02215, USA
e-mail: Patrick_Wen@dfci.harvard.edu

D. Schiff et al. (eds.), *Cancer Neurology in Clinical Practice*,
DOI 10.1007/978-3-319-57901-6_2

Table 2.1 Imaging differential diagnosis for intra-axial mass(es)

	Multifocal enhancing lesions	Solitary enhancing lesion
Solid	Metastases Multifocal glioma Lymphoma Demyelination Granulomatous disease	High-grade glioma Metastases Lymphoma Medullublastoma Ependymoma
Cystic	Metastases Infection (bacterial, fungal, parasitic)	High-grade glioma Metastases Hemangioblastoma Pilocytic astrocytoma Ependymoma
Calcification	Granulomatous disease Metastases (squamous cell carcinoma, mucinous adenocarcinomas, osteosarcoma, chondrosarcoma)	Oligodendrogliomas Gangliogliomas Central neurocytomas
Hemorrhage	Metastases (melanoma, renal cell carcinoma, and thyroid carcinoma) Fungal septic emboli	High-grade glioma Metastasis Pleomorphic xanthoastrocytoma

Tumor Permeability and Peritumoral Edema

Metastatic tumors to brain resemble the tissue characteristics of the primary tumors and therefore do not possess the blood–brain barrier seen in normal brain tissues. Thus, lesional enhancement is almost always observed for metastases on delayed post-contrast CT or T1-weighted MR images due to extra-vascular leakage of contrast agents. Aggressive primary intra-axial tumors such as higher grade astrocytomas, primitive neuroectodermal tumors, and primary CNS lymphomas also commonly enhance, although the mechanism of enhancement often include disruption of blood brain barrier and secretion of vasoactive substances. Other non-neoplastic intracranial processes can also exhibit contrast enhancement, including infarct, inflammation or infection.

One consequence of increased vascular permeability is accumulation of interstitial water content, resulting in decreased attenuation on CT as well as hyperintense signal on T2-weighted MRI from prolonged T2 relaxation times. A vasogenic pattern is characterized by edema that does not violate the boundary at the gray-white matter junction and can be easily identified by noting the exaggerated difference between gray and white matter attenuation or signal intensities on both CT and MRI. In contrast, cytotoxic edema resulted from direct damage to tissues as seen with ischemic infarction, does not spare the gray matter and there is a reduction in visual contrast at the gray-white matter junction. The extent of edema surrounding intra-axial metastases is often significantly greater than the actual tumor size. Rarely, vasogenic edema can be absent particularly with very small tumors (<1 cm).

When untreated brain metastases in the cortex near cerebral sulci or cerebellar folia are observed without associated edema, involvement of the extra-axial space, i.e. leptomeninges, should be suspected. Extra-axial metastatic tumors, similar to some meningiomas, can produce edema in the adjacent brain due to mass effect causing venous congestion or direct effect on capillary permeability.

Intratumoral Hemorrhage

Among intracranial metastases, hemorrhage more commonly occurs in melanoma, renal cell carcinoma, and thyroid carcinoma. Hemorrhagic metastases demonstrate variable signal intensities depending on the age of hemorrhage, and intratumoral hemorrhages tend to evolve more slowly and often contain blood product of mixed ages as compared to hemorrhages from non-tumor causes. Due to their intrinsic melanin content and frequently intratumoral hemorrhages, hyperintensity on unenhanced T1-weighted images can be observed in melanoma [5–7] (Figs. 2.1a–c and 2.2a–d).

Assessing whether parenchymal hemorrhage in brain is spontaneous or secondary to aneoplastic process is an important task in neuroimaging. Important clues to an underlying tumor include presence of nodular enhancement adjacent or within hematoma, incomplete hemosiderin ring, peritumoral edema more extensive than expected for the age of the hemorrhage, and delay in the expected evolution of signal characteristics in the hematoma. When these imaging signs are not present, short-term follow-up imaging may be required to confirm the nature of hemorrhage.

Venous infarcts can mimic a brain mass with enhancement, vasogenic edema, and hemorrhage. The site of sinus or cortical vein thrombosis can lead to venous infarct in corresponding venous drainage territory. Thus, recognizing

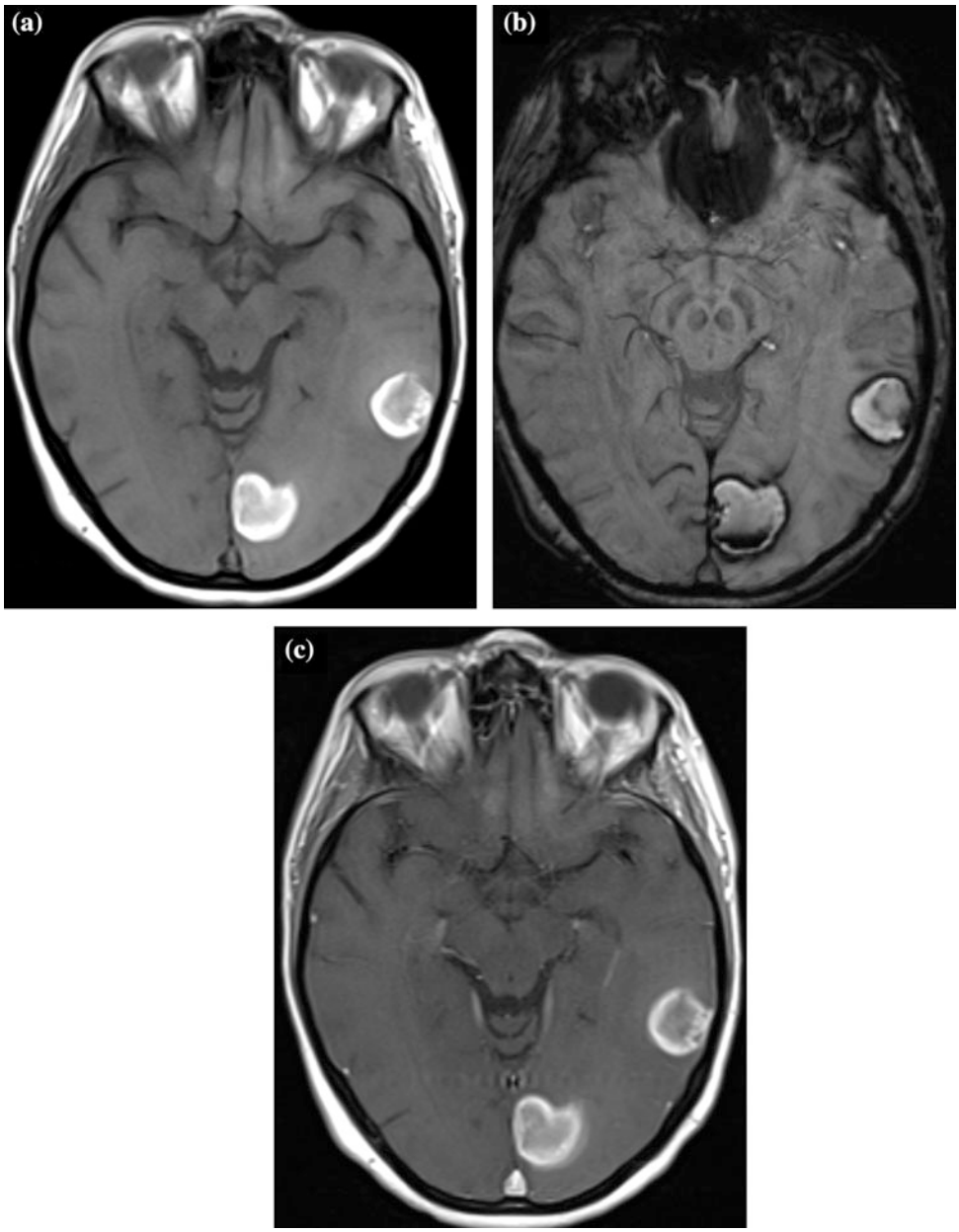

Fig. 2.1 **a–c** Melanoma hemorrhage. Two melanoma metastases in the *left* temporal and occipital lobes demonstrate hyperintensity on T1-weighted image (**a**). Following contrast administration, subtle enhancement is seen along the margins of hemorrhage. Magnetic susceptibility within the masses confirm presence of hemorrhage (**c**)

common location of venous infarct corresponding to site of thrombosis can be helpful in making the diagnosis.

Tumor Necrosis and Tumor Associated Cysts

Necrosis is a common imaging feature in brain metastases but also commonly seen with glioblastomas as well as lymphoma in immunocompromised population. Necrosis in metastases can also commonly occur following chemo- or radiation treatment, occasionally accompanied by enlargement of overall tumor size requiring close imaging follow-up to determine durability of treatment response.

Cystic brain metastases are commonly found with tumors of gastrointestinal or genitourinary origins but also occur in lung cancers [8]. In contrast to necrosis, tumor associated cysts tend to have thinner borders. Other primary neoplasms, including hemangioblastoma, pilocytic astrocytoma, and ganglioglioma can contain cysts although these tumors are usually not associated with peritumoral edema. Unlike post-chemotherapy or radiation necrosis often observed during treatment response, enlargement of tumor associated cysts often indicates elevated tumor secretion and can be a sign of tumor growth.

The thin-wall cysts seen in some metastases can appear identical to non-neoplastic cystic brain lesions. It is

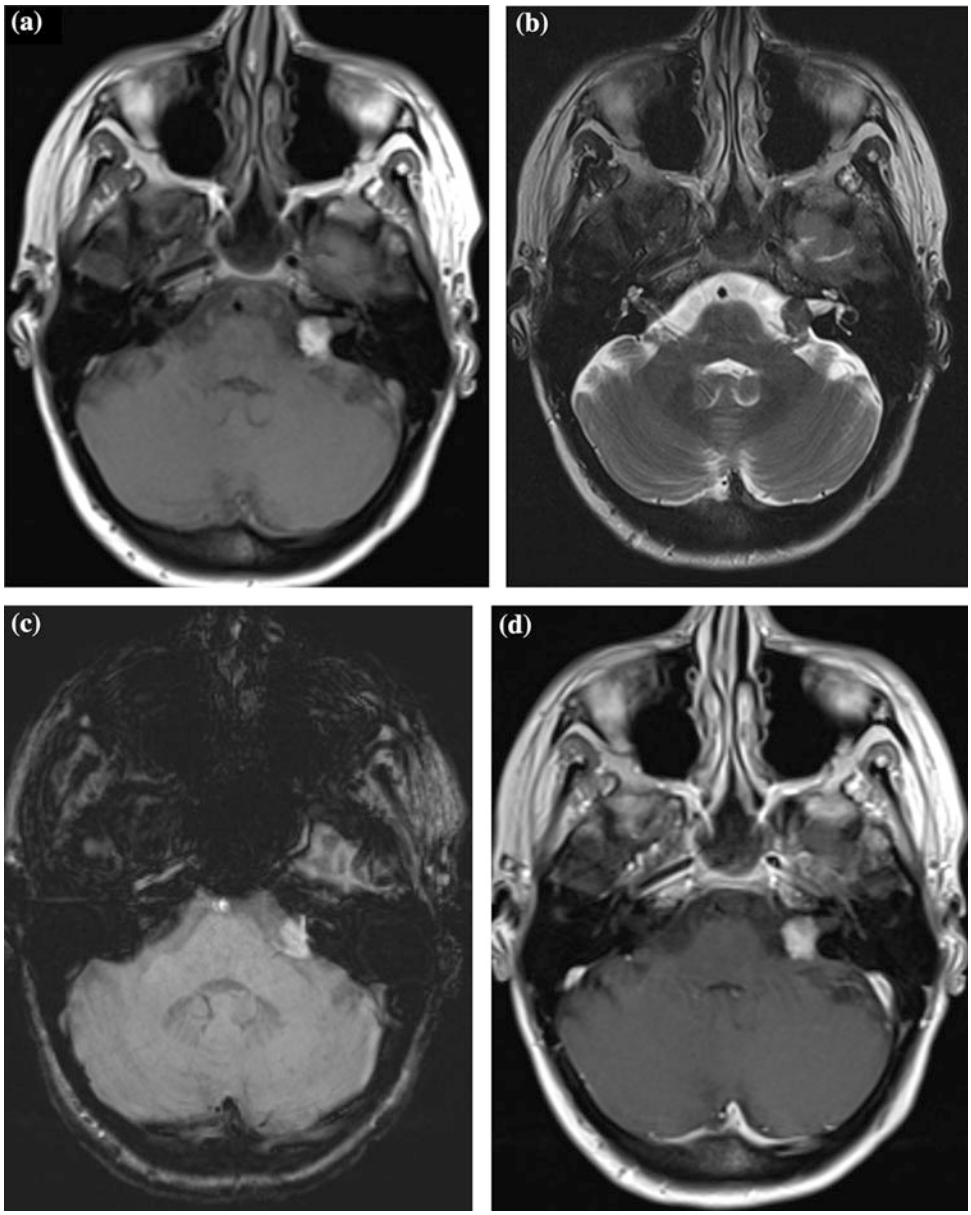

Fig. 2.2 **a–d** Melanoma. 33-year-old female presented with history of melanoma presenting with rapid onset hearing loss. A nodular lesion in the *left* cerebellopontine angle is hyperintense on T1-weighted image (**a**) and hypointense on T2-weighted images (**b**). No magnetic susceptibility is seen associated with this lesion (**c**). Following contrast administration, an enhancing component is difficult to detect in the presence of underlying T1 hyperintensity (**d**)

important to consider infectious etiologies such as brain abscesses, which can appear as multifocal rim-enhancing lesions and exhibit surrounding vasogenic edema. Often patients with brain abscess(es) have a distinct clinical history as well as presenting signs and symptoms from those with brain metastases, although it can be challenging to distinguish them clinically on occasions. Diffusion-weighted imaging based on the detection of changes in the random motion of protons in water is particularly helpful in diagnosing brain abscesses since their mucopurulent content tends to have very low diffusivity and exhibits a dark signal on the apparent diffusion coefficient (ADC) maps. In contrast, brain metastases have peripheral low diffusivity due to higher cell density while the necrotic content centrally tends to be of high diffusivity (bright on ADC). However, presence of hemorrhage can affect diffusion characteristics and one should be careful when there is evidence of susceptibility changes within the area of diffusion signal abnormality. Compared to abscesses, metastases are much more likely to be associated with hemorrhage. Furthermore, a small group of metastases, usually from GI or GU origins, may present as mucin-containing cystic lesions that manifest as similarly low diffusivity. On the other hand, atypical infections such as toxoplasmosis may not show low diffusivity within the cyst content.

Calcifications

Intratumoral calcifications rarely observed among untreated brain metastases, although it has been reported in a variety of tumor types, including common tumor metastasizing to brain such as lung and breast cancers as well as more rare tumor types including squamous cell carcinoma, mucinous adenocarcinomas from genitourinary or gastrointestinal origins, osteosarchoma, and chondrosarcoma [9, 10]. On the other hand, calcifications frequently occur in many primary intracranial tumors, most notably oligodendrogliomas, gangliogliomas, neurocytomas, and craniopharyngiomas. Following treatment, calcifications can develop within metastases. CT is both sensitive and specific in detecting macroscopic calcification, and approximately 3% of brain metastases seen on CT exhibited calcification in one series [11]. On MRI, calcifications can result in variable signal intensities depending on the microenvironment of calcium, but most commonly they appear as focal T1 shortening and magnetic susceptibility. These MR imaging findings, however, overlap with iron within blood products although they can be distinguished by differences in phase shifts [12].

Extra-Axial Intracranial Metastases

Within the extra-axial compartment metastases can involve bony structures of calvarium and skull base, dura (pachymeninges), leptomeningeal spaces including cerebral sulci, cerebellar folia, and cranial nerves, or within ventricles. Similar to osseous metastatic tumor elsewhere, metastases to calvarium and skull base can have lytic, sclerotic, or mixed patterns on CT depending on primary tumor subtypes. For example, prostate cancer metastases are generally sclerotic, whereas renal and thyroid metastases tend to present as lytic lesions. Following treatment, lytic metastases frequently produce a sclerotic pattern.

Dural (pachymeningeal) metastases often grow from adjacent calvarium or skull base but can be directly seeded from hematogeneous sources. Breast cancer, lymphoma, leukemia, prostate cancer, and neuroblastoma are tumors most commonly presenting as dural metastases (Fig. 2.3a–c). Meningiomas are the most common benign tumor arising from dura, and it can be difficult to distinguish from dural metastases unless meningiomas contain calcifications or induce hyperostosis of adjacent bone. Intracranial hypotension is a common non-neoplastic cause of dural enhancement but the pattern of enhancement is almost always diffuse and smooth rather than focal or nodular, and is often supported by clinical history of previous cranial or spinal intervention. In severe cases, intracranial hypotension can be associated with subdural hygroma or hematoma, and it is also not uncommon for dural metastases to produce subdural fluid collection or hemorrhage. Contrast-enhanced MRI is best for detecting nodular enhancement along the dural lining of hematomato diagnose dural-based tumor (Fig. 2.3a–c).

Leptomeningeal metastases occur in many types of cancer, particularly breast carcinoma, lung carcinoma, melanoma, lymphoma, and leukemia. Metastatic spread to the meninges can occur hematogenously via meningeal vessels or through direct extension from metastatic lesions at the pial surface. Leptomeningeal metastases are usually not detectable on CT without contrast enhancement, although hydrocephalus can be an indirect sign of leptomeningeal involvement. Contrast-enhanced MRI provides significant better sensitivity in detecting leptomeningeal metastases as planar or nodular enhancement along cerebral sulci, cerebellar folia, or cranial nerves [13] (Fig. 2.4a–c). Other non-tumor processes including ischemic infarction and leptomeningitis can also exhibit enhancement along brain surfaces but often can be distinguished based on clinical history. A nodular pattern of leptomeningeal enhancement is more commonly seen with neoplastic processes but can also be observed in infectious etiologies. CSF analysis should be obtained when leptomeningeal abnormality is identified on imaging but there is uncertainty regarding the diagnosis. On fluid-attenuated inversion recovery (FLAIR) sequence, leptomeningeal tumor can appear as hyperintense signal along sulci as a result of shortened T1 relaxation time but this finding without enhancement is not specific since other CSF pathologies such as hemorrhage or infection can appear identical. Unlike parenchymal metastases, leptomeningeal seeding of tumor commonly does not lead to significant vasogenic edema, although edema and mass effect can be observed when there is florid involvement. Table 2.2 summarizes the main differential diagnoses of extra-axial masses.

General Approach to Imaging of Patients Presenting with Suspected Brain Metastases

When one or more enhancing mass is found on brain imaging of a patient with known progressive or recurrent metastatic cancer, diagnostic certainty for brain metastasis is high. For patients with no or remote history of cancer presenting with newly discovered brain mass(es), the diagnostic possibilities can be broad, including primary brain neoplasms, infection, demyelinating lesions, vascular lesions that can be difficult to distinguish from brain metastasis on both imaging and clinical presentation.

While multiplicity can be helpful in making the diagnosis, solitary metastases are common and can be difficult to distinguish from other intra-axial tumors such as primary glioma or lymphoma, as well as non-neoplastic mass-like

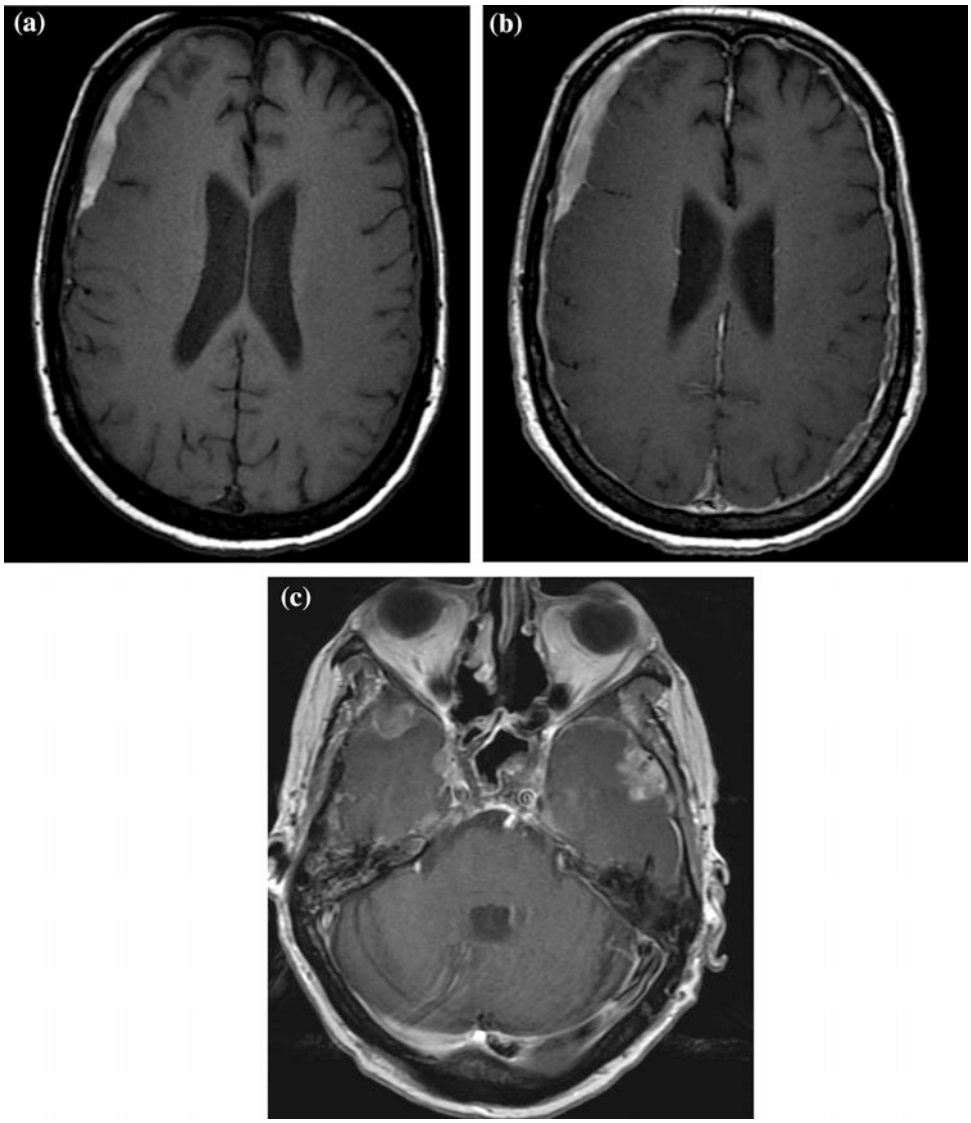

Fig. 2.3 **a–c** 70-year-old man with metastatic prostate cancer presents with headache. T1-weighted unenhanced image shows a T1 hyperintense collection along right frontal convexity (**a**) consistent with subacute subdural hematoma. Following intravenous contrast administration, extensive dural thickening with multifocal enhancing masses are identified (**b** and **c**), evening along the lining of subdural hematoma (**b**)

processes such as demyelination, infection, or vascular pathology. When multifocal enhancing brain metastases occur, the extent of T2 signal abnormality surrounding lesions tend to be separated on T2-weighted imaging, whereas multifocal enhancement in high-grade gliomas typically show contiguous areas of infiltrative appearing nonenhancing T2 abnormalities between foci of enhancement. In addition, the areas of T2 abnormality in high-grade glioma often demonstrate infiltration of gray matter.

Demyelination disease can be "tumefactive," mimicking a brain mass clinically and on imaging. These lesions, however, tend to occur in younger patients without history of malignancy. On imaging, an "incomplete ring sign" is an important feature suggesting the presence of a demyelinating lesion. CSF analysis for gamma globulin can help clarify the diagnosis, and follow-up imaging several months later often confirms eventual improvement or resolution.

Vascular lesions including arterial or venous infarction as well as vascular malformations can mimic a brain mass. Ischemic infarcts, particular during subacute phase, can present as enhancing lesions 2–3 days following onset of the ischemic event that persist for several months; diffusion signal changes typically associated with acute infarct usually normalize after 7–10 days [14]. Enhancement associated with ischemic infarct, however, does not exhibit surrounding vasogenic edema. For small enhancing lesions along gray matter that cannot be diagnosed as infarction based on clinical history or lesion location, a short-term follow-up imaging can readily clarify the etiology. It is important to keep in mind that ischemic infarct can coexist with brain metastasis due to a hypercoagulable state associated with malignancy, as well as from embolic events from systemic procedures. In addition, perioperative infarct is not infrequently observed and often located immediately adjacent to

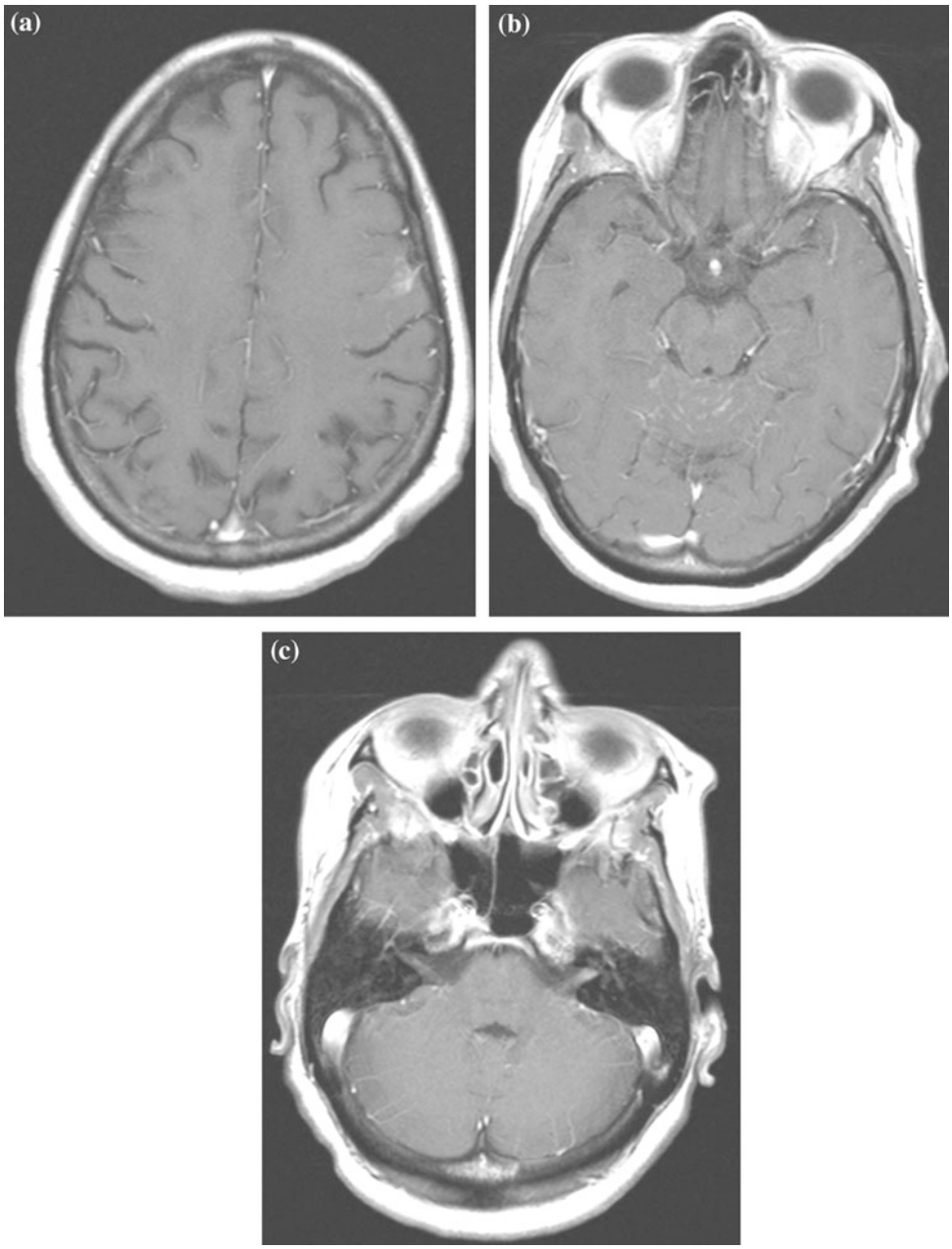

Fig. 2.4 **a–c** Leptomeningeal. 55-year-old man with history of lung cancer presents with acute headache and gait disturbance. Axial T1-weighted post-contrast images demonstrate leptomeningeal carcinomatosis with enhancement along cerebral sulci (**a**), cerebellar folia (**b**), and cranial nerve in the internal acoustic canals (**c**)

Table 2.2 Differential diagnosis for extra-axial mass(es)

Intraosseous-calvarium	Leptomeningeal	Pachymeningeal
Hemangioma	Metastases	Meningioma
Fibro-osseous lesions	Infectious meningitis	Metastases
Metastasis	Lymphoma	Lymphoma
Langerhans cell histiocytosis	Sarcoidosis	Sarcoidosis
Sarcoma	PNET	Idiopathic pachymeningitis
Meningioma		

the surgical margin. It is important to perform and examine the diffusion- weighted sequence during the immediate postoperative MRI to identify area(s) of peritumoral infarct so the expected subsequent enhancement will not be misinterpreted as tumor recurrence.

When brain imaging reveals findings suggestive of metastatic disease in a patient without history of systemic cancer, imaging for potential primary cancer site or additional extracranial metastases is often necessary to identify an anatomical site that carries a lower risk for diagnostic

biopsy. The imaging modalities depend on the patient demographics, but often include CT scan of the chest, abdomen and pelvis. FDG-PET imaging can be highly sensitive in detecting occult primary malignancy and can be used as part of staging in many systematic cancers.

Optimization of Radiological Protocol for Evaluation of Intracranial Metastasis

For staging systemic malignancy in an asymptomatic patient, CT can be the test of choice due to its wider availability and the speed of imaging. While small brain metastases can be difficult to detect by CT unless there is significant surrounding edema, mass effect or intratumoral hemorrhage, CT has the advantage of visualizing lesions that are centered in bone or producing calcifications. CT imaging of the bony margins can help elucidate the underlying pathology. For example, slow-growing lesions are often accompanied by bone remodeling and manifesting as smooth cortical rather than destructive margins. Calcifications are often found in a subset of brain tumors, including meningioma, oligodendroglioma, germ cell neoplasm, and craniopharyngioma, and these are better visualized by CT evaluation. CT may be the only available option for screening if patients have contraindications for MRI such as cardiac pacers, ferromagnetic foreign bodies, implants or surgical devices. While whole-body ^{18}fluoro-D-glucose positron emission tomography (FDG-PET) is commonly used for initial stating of systemic cancers, its sensitivity in detecting brain metastases is generally considered low due to relative high FDG uptake in normal brain tissues. For example, the sensitivity of brain PET/CT for detecting brain metastases in lung cancer was 72% in one series [15].

For most systemic malignancy, MRI is the imaging modality of choice in assessing brain metastases due to its excellent soft tissue contrast and lack of ionizing radiation. Several MRI sequences are generally recommended during evaluation of brain metastases. An isotropic volumetric post-gadolinium T1-weighted sequence allows detection of very small lesions, on the order of 1–2 mm. This high sensitivity can be important since the total number as well as the distribution of metastatic brain lesions contributes to selection of treatment approach. The sensitivity of detecting brain metastasis can be improved by increased time duration following contrast and using contrast agents with longer T1 relaxation time [16–18]. Higher magnet strengths, i.e., 3 versus 1.5 T, can further increase sensitivity [19, 20]. In addition, volumetric acquisition allows multi-planar reformation for better lesion visualization and can be fused with stereotactic equipment for surgical guidance. This type of acquisition method requires longer acquisition time and is therefore more susceptible to patient motion artifact when performed using lower field strength MR scanners. Finally, it is often helpful to perform a T1-weighted sequence before contrast administration to distinguish true enhancement from other tissue types with short T1 relaxation times such as hemorrhage, fat or proteinaceous cyst.

Mass lesions with a cystic component as well as perilesional edema can be readily delineated by a T2-weighted sequence. Infiltration of tissues with prolonged T2 relaxation time in the cortical gray matter with expansion of gray matter and blurring of the gray-white matter junction is a specific sign of primary glioma and not observed with metastatic tumors. On T2-weighted imaging, the interface of tumor and adjacent brain often appears sharper compared to high-grade gliomas.

Diffusion weighted imaging (DWI) is commonly included during evaluation of brain lesions due to its high sensitivity in detecting a variety of brain pathologies including infarct, abscess, cerebritis, and tumor that manifest as hyperintensity on DWI and hypointensity on apparent diffusion coefficient (ADC) maps that are calculated from DWI. Findings on DWI images are more helpful when they are interpreted alongside conventional imaging sequences and clinical history for improved specificity. For example, subacute infarct can manifest as cortical swelling and enhancement mimicking brain tumor, but a serpiginous pattern of low diffusivity confined to an arterial distribution is characteristic of ischemic infarct rather than neoplasm. When a peripherally enhancing brain lesion is encountered, evidence of low diffusivity within the lesion is suggestive of abscess as discussed previously but the diagnostic specificity can be increased if the enhancing rim is also thin and systemic signs of infection are present.

On MR imaging, DWI has also been correlated with hypercellularity typically manifesting as reduced diffusivity on the ADC map [21]. This imaging marker of cell density can be used to help several tumor types that are characteristically hypercellular, including breast and lung metatases [22]. CNS lymphomas are characteristically cellular [21, 23] and are more commonly located in the periventricular regions of brain. It is important to recognize that intratumoral hemorrhage can appear as hyperdensity on CT, and ADC measurement can also be decreased due to presence of blood product. DWI is also very useful in identifying calvarial and skullbase metastases due to its high lesion to background contrast [24] (Fig. 2.5a, b).

T2*-sensitive techniques such as gradient-echo and susceptibility-weighted imaging are useful for detecting intratumoral hemorrhage, which is common in high-grade gliomas and metastases, but rare in low-grade gliomas and

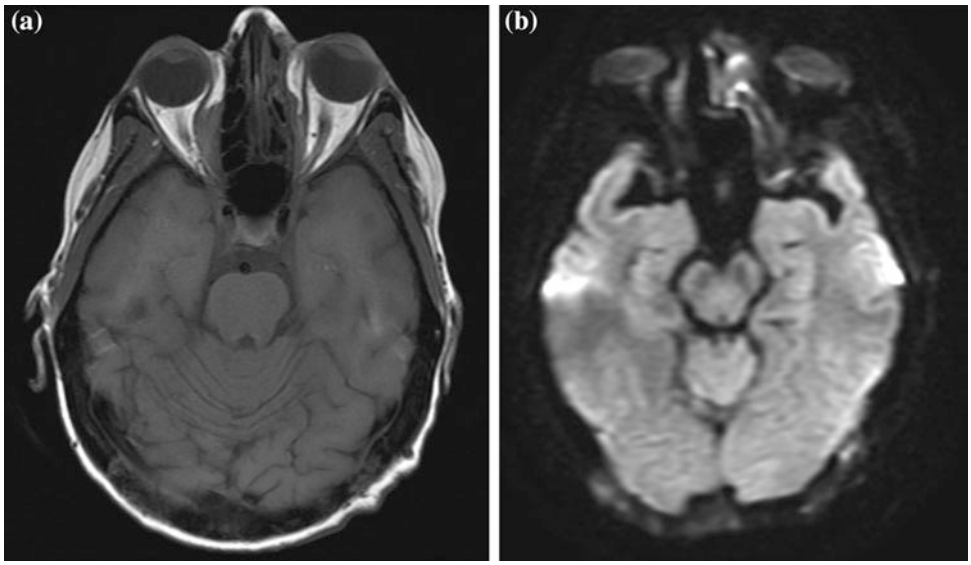

Fig. 2.5 **a–b** DWI-Calvarium-Orbit. 46-year-old female with breast cancer developed metastases to calvarium and right orbit. The lesions are seen on both T1-weighted imaging (**a**) than DWI (**b**), although more conspicuous on the latter due to greater lesion to background contrast

lymphoma. The deoxyhemoglobin causes magnetic susceptibility that results in shortened T2* relaxation times and hypointense signal changes on T2*-weighted (T2*W) images. This phenomenon can improve sensitivity of detecting small metastatic lesions with hemorrhages that do not enhance or elicit peritumoral edema. For example, 7% of melanoma lesions were detected only on this sequence in one series [5]. Susceptibility-weighted imaging (SWI) can amplify the effect of magnetic susceptibility by overlaying magnetic phase changes with high-resolution magnitude images to detect foci of microhemorrhages [25]. These techniques are also helpful in identifying thromboses within dural venous sinuses or cortical veins due to exaggerated magnetic susceptibility from deoxyhemaglobin [26]. The appearance of venous infarction on conventional MRI sequences can mimic brain tumor due to mass effect, edema, and enhancement. If misdiagnosed, this can lead to unnecessary biopsy or a delay in anticoagulation treatment.

Advanced Techniques in Brain Metastasis Imaging

Several imaging techniques have become increasingly available for evaluation of brain lesions including MR spectroscopy, MR perfusion, and MR diffusion tensor imaging. When combined with conventional imaging sequences, these advanced methods can often provide useful diagnostic information when evaluating brain lesions including metastases. As these advanced imaging methods are being improved and validated, it is important to understand their advantages and limitations before incorporating them into clinical imaging protocol.

Magnetic Resonance Spectroscopy (MRS)

MR spectroscopy can provide a noninvasive window to analyze metabolic composition of brain lesions. Similar to most pathological processes observed in brain, metastases show reduced NAA peak on MR spectroscopy [27, 28], and the level of NAA concentration is often absent or much lower than other intrinsic brain pathologies where brain tissues are being infiltrated or damaged as in case of primary brain tumor or inflammation. Choline concentration also typically increases in the enhancing portion of metastases as a result of increased cellular turnover [27, 29]. This metabolic marker can be useful in distinguishing peritumoral edema surrounding metastases from infiltrative glioma since reactive or vasogenic edema, unlike tumor infiltration, does not result in greater cellular turnover [30]. Lipids and lactate are also frequently seen in metastases although these are not specific findings and can be found also in high-grade gliomas [30]. Based on a retrospective analysis of multicenter trial data, automatic brain tumor classification by MRS allows classifications of glioblastoma, meningioma, metastasis, and low-grade glial with diagnostic accuracies of near 90% for most diagnostic pairs except for the glioblastoma versus metastasis discrimination [31].

Perfusion-Weighted Imaging (PWI)

Similar to high-grade primary brain neoplasms, metastatic lesions induce neovascularization resulting in greater intravascular blood volume, although the vessels associated with metastases are highly permeable similar to those of the primary systemic tumors [32]. Estimation of intravascular volume in tumors can be performed by dynamic imaging methods such as dynamic contrast-enhanced MRI (DCE-MRI), dynamic susceptibility contrast MRI (DSC-MRI), as

well as dynamic contrast-enhanced CT. Due to its short acquisition time of less than 2 min, DSC-MRI can readily be incorporated into standard imaging protocol for evaluation of brain mass. Elevation of regional cerebral blood volume (rCBV) is characteristic of most high-grade gliomas, although metastatic tumors, particularly renal cell carcinoma, choriocarcinoma, and thyroid carcinoma, can also demonstrate high intravascular blood volume making this diagnostic imaging marker less useful [33]. The specificity of DSC-MRI can be improved by using spin-echo (SE) acquisition compared to gradient-echo (GRE) since the former technique appears to correlate with microscopic angiogenesis that is typical with gliomas, while the later technique detects macroscopic intratumoral vessels more commonly seen in cases of hypervascular metastases [34]. Furthermore, higher rCBV within the peritumoral region is also suggestive of infiltrative tumor rather than vasogenic edema [35, 36].

Diffusion Tensor Imaging (DTI)

The magnitude and directionality of water motion can be quantified by DTI and used as imaging markers to characterize microstructural changes occurring at tissue or cellular levels [37]. This technique can be highly sensitive to pathological changes in brain including both neoplastic and non-neoplastic processes, although its specificity is low without advanced post-processing. For example, fractional anisotropy (FA) values of high-grade gliomas and solitary brain metastases show significant overlap [38, 39]. Similar to

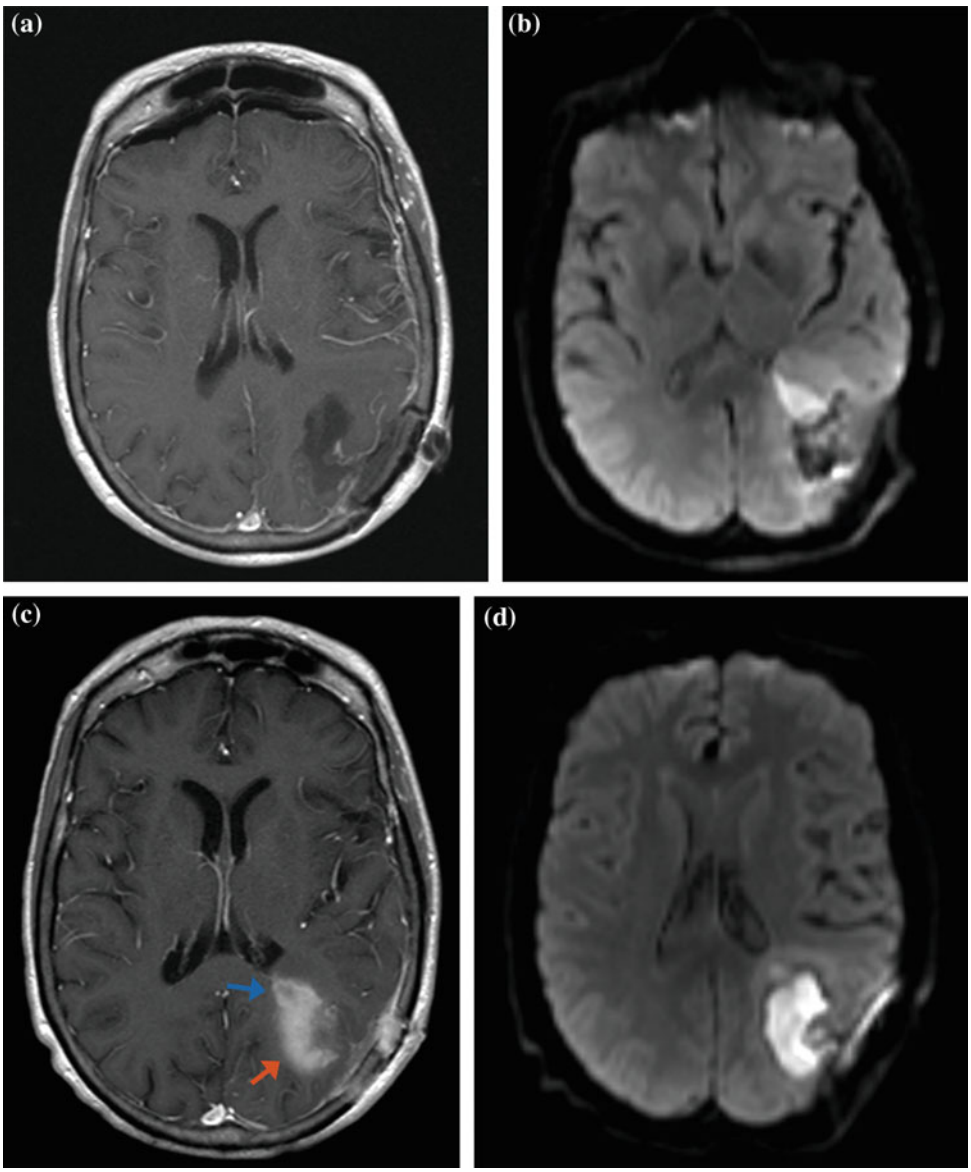

Fig. 2.6 **a–d** Infarct. 48 h postoperative MRI demonstrates no significant enhancement near resection bed on contrast-enhanced T1-weighted image (**a**) but a wedge-shaped DWI abnormality anterior to the resection cavity (**b**). **b** Two weeks following surgery, the regions of previous infarct exhibit enhancement (**c**) (*blue arrow*) with normalization of DWI abnormality (**d**), and the blood product within resection cavity appears hyperintense on T1-weighted image (**c**) (*red arrow*) and bright on DWI (**d**)

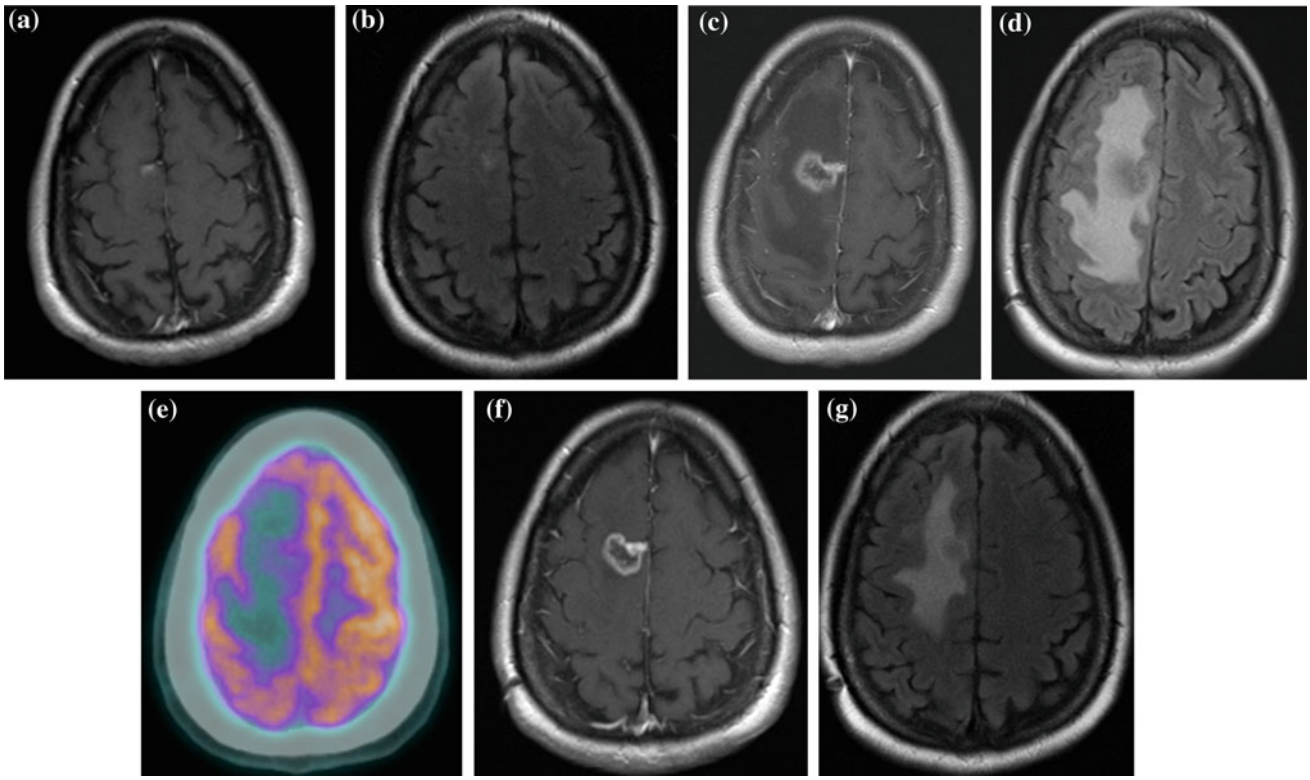

Fig. 2.7 **a**–**g** Radiation necrosis. 51-year-old woman with history of breast cancer and brain metastatic received SRS treatment to a superior *right* frontal lesion. Axial enhanced T1W and FLAIR images at one month (**a** and **b**) and 9 month (**c** and **d**) following treatment, demonstrating interval increase in size of enhancement and surrounding edema. FDG-PET shows no significant uptake in the region of enhancement relative to adjacent brain (**e**). At 15 months after treatment, the area of enhancement and surrounding edema decreased in size (**f** and **g**)

Table 2.3 Differential diagnosis for spinal mass(es)

	Multifocal enhancing lesions	Solitary enhancing lesion
Extra-dural	Metastasis Lymphoma Myeloma Granulomatous disease	Metastasis Meningioma Schwannoma Neurofibroma Lymphoma Myeloma/plasmacytoma
Intradural, extramedullary	Metastasis (systemic or CNS origins) Schwannomas Neurofibromas Granulomatous disease	Schwannomas Neurofibromas Metastasis
Intramedullary	Demyelinating disease Hemangioblastomas Metastasis Abscesses Granulomatous disease	Ependymoma Astrocytoma Hemangioblastoma Demyelinating disease Metastasis

PWI and MRS, measuring peritumoral nonenhancing abnormalities result in improved specificity [38, 40]. More recently, using k-means clustering of FA/mean diffusivity (MD) data, metastasis can be differentiated from high-grade glioma and meningioma with high accuracy [41].

Morphological Analysis

While qualitative assessment of tumor morphology based on MR imaging can contribute to diagnosis of brain tumors, the subjective nature of such evaluation methodology introduces

significant variability. More recently, quantitative approaches to these imaging features have been developed. Three-dimensional (3D) shape morphology of tumor has been used to build morphometric models of glioblasdtomas and brain metastases pathology [42, 43]. These promising techniques require further validation using larger prospective imaging data. Once validated, software optimization will also be necessary prior routine clinical use.

Post-therapeutic Evaluation of Brain Metastasis

In order to assess presence of residual tumor, postoperative MRIs are usually performed within 48 h following surgical resection prior to onset of enhancement along surgical margins [44, 45]. During this period, enhancement is highly suggestive of residual tumor. In addition, perioperative brain infarction can be detected during early postoperative

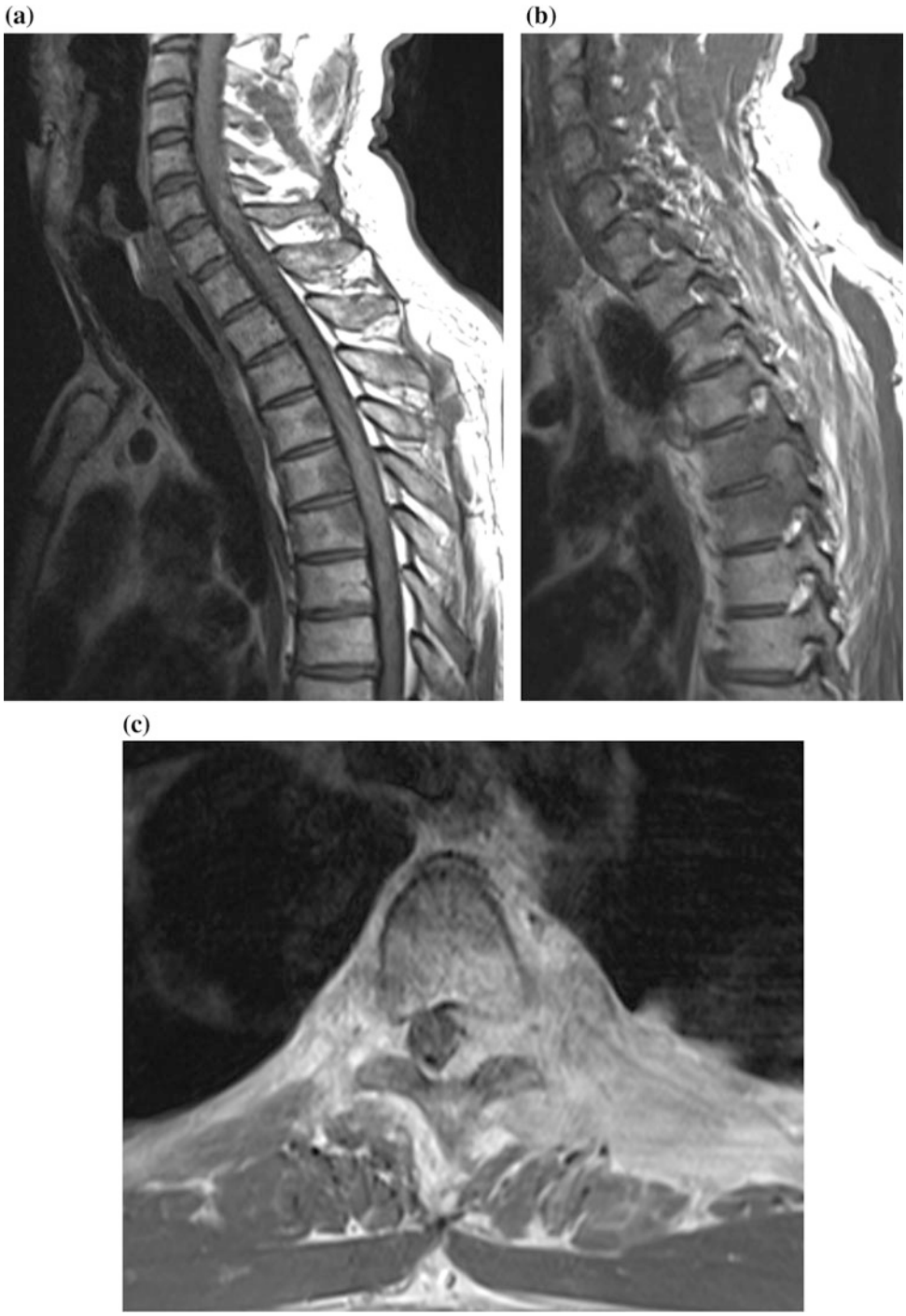

Fig. 2.8 **a–c** Spine epidural. 45-year-old male with lung cancer presents with back pain. Sagittal T1 weighted image without contrast enhancement (**a**) shows abnormal marrow signal in the posterior aspect of multiple vertebral bodies in the thoracic spine. Sagittal T1-weighted image without contrast enhancement (**b**) and axial T1W post-contrast image (**c**) show involvement of *left* epidural space and neural foramen with narrowing of thecal sac and flattening of spinal cord

imaging with diffusion weighted imaging. Documenting presence of infarction can be important since enhancement from evolved infarction can mimic tumor residual tumor [14] (Fig. 2.6a–d).

Increased enhancement along surgical margins can also occur during postoperative infection. Enlargement of surgical cavity and increased degree of surrounding edema are suspicious signs for infection. While low diffusivity on diffusion-weighted imaging is a specific imaging sign of an abscess, a small number of brain metastases also exhibit low diffusivity and this finding is also less specific in the postoperative setting in the presence of evolving blood products within resection cavity [46] (Fig. 2.6a–d).

Depending on number, location and types of brain metastases, focal or whole brain radiation therapy is commonly performed alone or following surgical resection. Not infrequently, brain injury following radiation can produce clinical and imaging findings that resemble tumor progression or recurrence. It is important to recognize a number of imaging patterns associated with radiation treatment to avoid unnecessary surgery or cessation of effective chemotherapy.

Radiation-related brain injuries can be categorized by their timing following therapy initiation into acute (within weeks), subacute (within 3–4 months) and late (4 months to years) phases. Acute radiation injuries are transient and can appear normal on imaging or show increased edema and contrast enhancement. Subacute and delayed radiation injuries are often accompanied by increased edema and enhancement at and around original tumor site that can mimic tumor progression (Fig. 2.7a–g). Seventy percent of focal late radiation injuries occur within 2 years after therapy. Demyelination of white matter in periventricular regions is also a common late manifestation of injury following whole brain radiation treatment, characterized by gradually increasing patchy-appearing areas of T2 prolongation without associated mass effect or enhancement. White matter volume loss as a result of radiation injury can be apparent from expansion of ventricular size, although communicating hydrocephalus can be a superimposed clinical imaging finding that may be difficult to distinguish without a shunt trial. Capillary telangiectasias and cavernous malformations are vasculopathies that often develop several years to decades after radiation therapy. These lesions can be readily recognized by multifocal small hemosiderin depositions on T2*-weighted imaging and are not associated with edema or mass effect [47].

While it is usually difficult to distinguish radiation necrosis from tumor recurrence, several imaging features

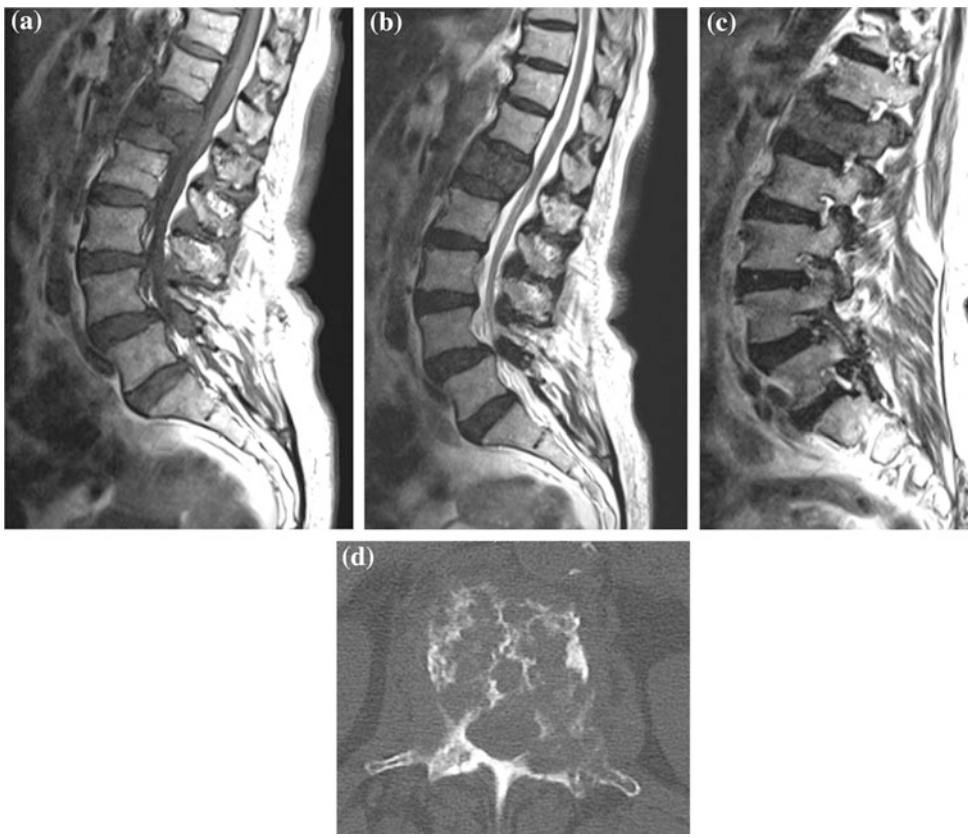

Fig. 2.9 **a–d** Pathological Fracture. 88-year-old female with history of breast cancer presents with back pain. Sagittal T1 (**a**) and T2 (**b**) weighted images show compression fracture of L1 vertebral body with abnormal marrow signal involving the entire vertebral body and there is a convex appearance of the posterior cortex. The posterior element also shows abnormal marrow signal (**c**). Trabecular and cortical destructions are readily identified on axial CT imaging (**d**)

have been observed to help distinguish the two. Following radiosurgery, longer time between radiosurgery and resection and a larger edema/lesion volume ratio are predictive of radionecrosis as opposed to tumor recurrence [48]. Delayed MRI at greater than one hour following contrast injection can differentiate tumor from non-tumor tissues with high sensitivity and positive predictive value to active tumor [49]. Texture features analysis of conventional MRI sequence also provides improved classification accuracy in differentiating brain metastasis and radiation necrosis [50].

Advanced MR imaging techniques including DWI, MRS, and PWI have been used to differentiate radiation necrosis following lesions treated by stereotactic radiosurgery [51]. Radiation necrosis usually shows heterogeneity on DWI images and has significantly higher maximal ADC values compared to recurrent tumors [52]. While the blood volume and blood flow measurements of brain metastases on PWI are highly variable depending on primary tumor histology, a change in PWI parameters between pre-treatment and post-treatment imaging provides greater diagnostic value; a decrease of rCBV values indicates radiation-induced necrosis while elevation of rCBV following treatment is indicative of tumor recurrence [53]. Based on serial change in the tissue choline/creatine level and lipid–lactate complex, MR spectroscopy can distinguish tumor recurrence from radiation-induced changes [54, 55]. While these advanced MR imaging techniques are undergoing validation for their clinical utility, they also require expertise in imaging quality control and postprocessing to ensure diagnostic consistency.

^{18}FDG PET can also distinguish between necrosis and recurrent tumor with modest accuracy raging from 50 to 70% [56, 57]. Residual or recurrent tumor usually demonstrates increased FDG uptake, whereas necrosis from radiation or chemotherapy usually demonstrates isometabolic or decreased FDG uptake, although there is significant overlap in the uptake values. Novel amino acid PET radiotracers with high lesion to background ratio have been evaluated for imaging of metastases. 6-[(18)F]-fluoro-L-3,4-dihydroxyphenylalanine (F-DOPA) PET can differentiate radionecrosis from tumor progression with greater overall accuracy compared to perfusion-MRI [58].

Finally, CNS metastases can respond to systemic treatment differently from tumors at extracranial sites secondary to differences in drug penetration, tumor genetic

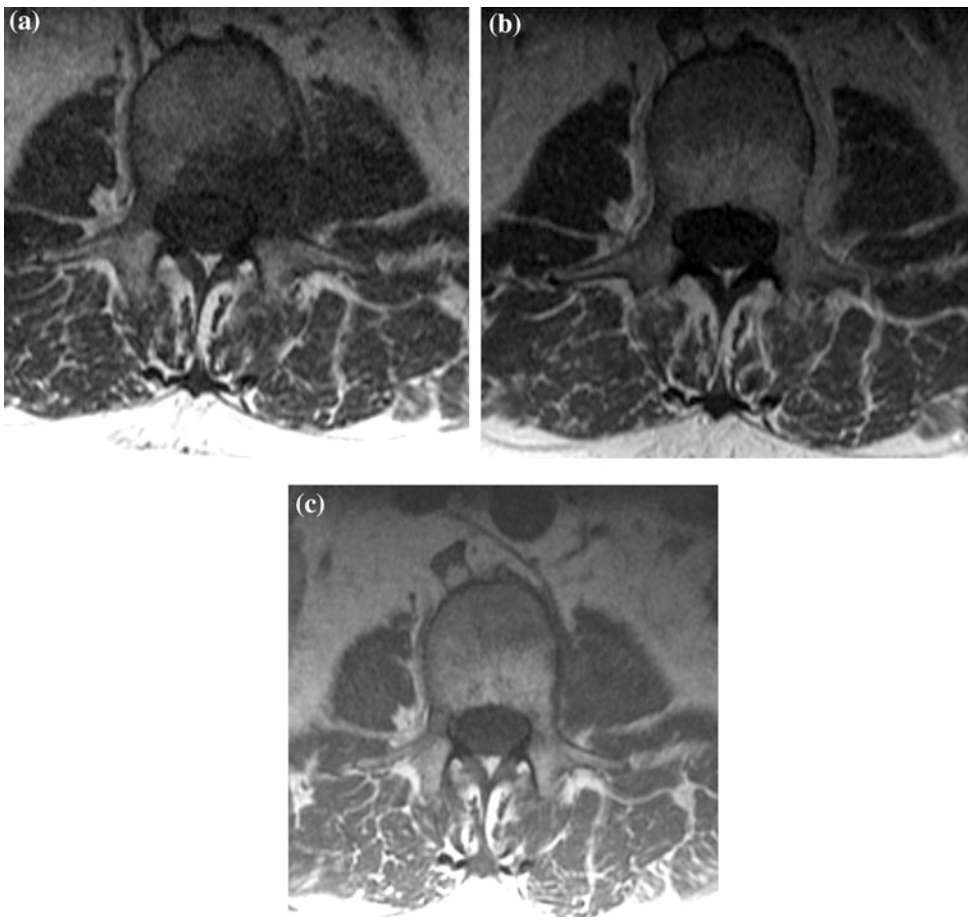

Fig. 2.10 **a–c** Hemangioma. 69-year-old with history of colon adenocarcinoma presented with new lumbar spine mass discovered on abdominal imaging. Axial T1-weighted images before (**a**) and after (**b**) intravenous contrast administration showed an enhancing mass involving the left aspect of vertebral body extending to pedicle and left paravertebral space. Percutaneous needle biopsy did not reveal malignant cells, and mass decreased in size without treatment on subsequent imaging, demonstrating characteristic hyperintensity of hemangioma on unenhanced axial T1-weighted image (**c**)

Fig. 2.11 **a–d** Spine intradural. 54-year-old male with metastatic melanoma presented with progressive right lower extremity weakness. Sagittal and axial T2- (**a** and **c**) and T1-weighted contrast (**b** and **d**) enhanced images show heterogeneously enhancing intradural, extramedullary mass resulting in leftward displacement and flattening of the spinal cord (**d**). There is cord edema on axial T2-weighted image (**c**)

heterogeneity, and tumor microenvironment. On the other hand, localized therapies for CNS lesions including whole brain radiotherapy and stereotactic radiosurgery can produce a local response despite progression of systemic disease. Therefore, two-compartment response assessment criteria has been proposed to account for both CNS and non-CNS tumor burden [59].

Spinal Metastasis

Metastases to the spine can also be classified by their anatomical locations with respect to the dura and involvement of the spinal cord (Table 2.3). Most commonly, metastatic spinal lesions are extra-dural, found predominantly in the vertebral bodies and posterior elements with

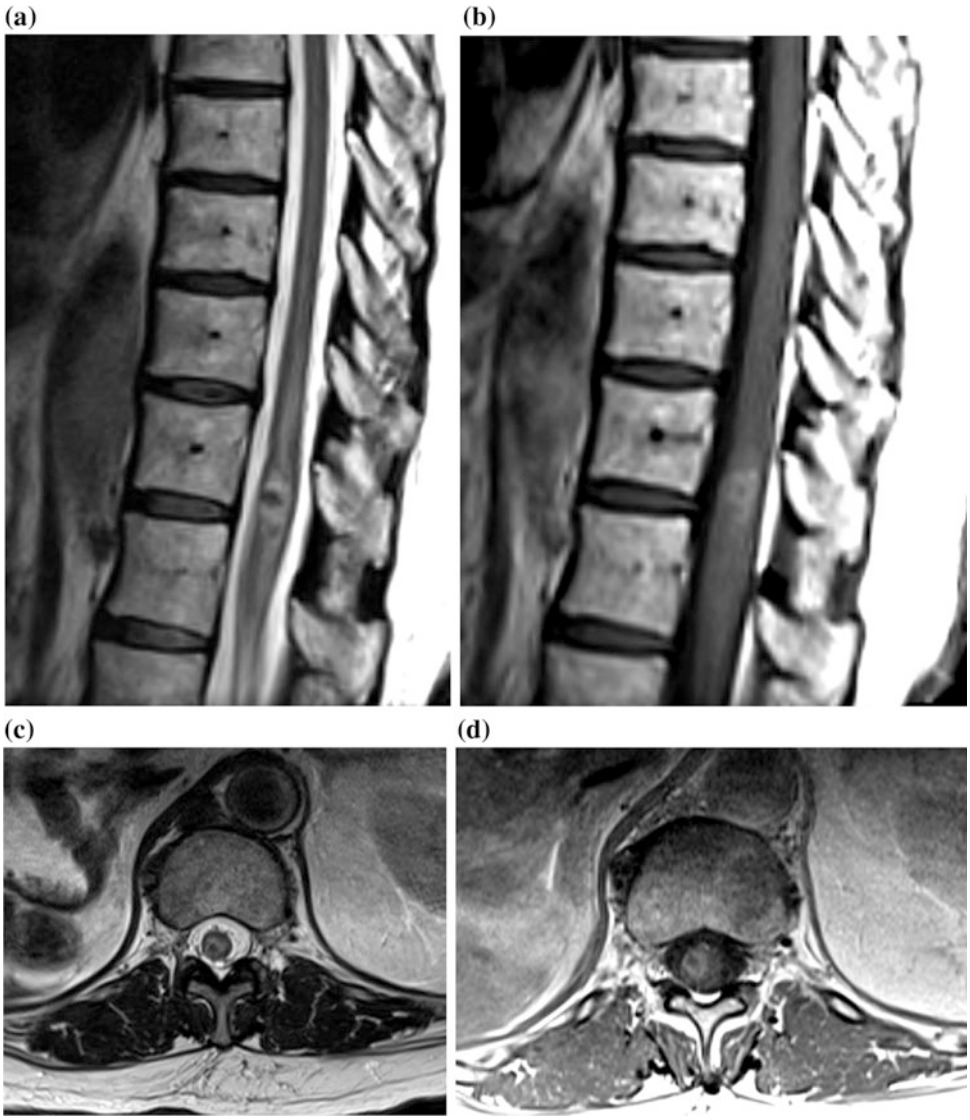

Fig. 2.12 **a–d** Intramedullary metastasis. 63-year-old female with renal cell cancer presents with intramedullary metastasis. Sagittal and axial T2-weighted images (**a** and **c**) show a solitary lesion with central hypointensity and surrounding edema. There is enhancement on post-contrast T1-weighted images (**b** and **d**)

frequent extension to the epidural compartment causing compression of spinal cord or nerve roots. Epidural spinal cord compression occurs in approximately 5% of patients with cancer [60]. MRI, in particular unenhanced T1-weighted imaging, is most sensitive in detecting marrow involvement and diagnosing epidural disease due to replacement of marrow and epidural fat (Fig. 2.8a–c). Flattening of spinal cord contour with or without edema suggests cord compression (Fig. 2.8a–c). While cord compression is usually a clinical diagnosis, imaging is important for confirming locations of tumor to facilitate surgical or radiotherapy planning. Since multiple spinal levels are often simultaneously involved, it is important to obtain imaging of the entire spine.

Occasionally it can be difficult to distinguish pathological vertebral fractures from insufficiency fractures. On MRI, preservation of normal marrow signal in the non-compressed portion of vertebra and linear fluid signal or vacuum favor non-tumor etiologies [61–63]. Retropulsed fracture fragments at the posterior vertebra, usually located at the superior endplate, is highly specific for a benign fracture but has low sensitivity [64]. On the other hand, abnormal marrow signal in the pedicle or posterior element suggests metastatic involvement [65] (Fig. 2.9a–d). A convex posterior border of the vertebral body is also commonly found in metastatic compression fractures [65] (Fig. 2.9a–d). Destruction of cortical bone of the vertebral body or the pedicle provides important clues to underlying malignancy and can be best visualized on CT (Fig. 2.9a–d). DWI methods has been used to differentiate benign from metastatic compression fractures and can improve diagnostic accuracy when added to conventional MR sequences [66–69].

Presence of paraspinal or epidural enhancing soft tissues as well as additional spinal metastatic lesions are signs of tumor involvement [70], although one must also consider fluid or soft tissue findings related to hematoma, infection, or

atypical hemangiomas. In particular, findings suggestive of vertebral height loss due to infection have contiguous vertebral, endplate and disk involvement.

Hemangiomas are common benign lesions in spine that are typically diagnosed on the basis of intrinsic short T1 (hyperintense) signal. However, a subset of hemangiomas exhibit atypical imaging appearances including lack of hyperintensity on T1-weighted images and aggressive changes including cortical disruption and epidural/paravertebral extension (Fig. 2.10a–c). Detection of a characteristic "polka dotted" trabellular pattern on both MRI and CT can be helpful in diagnosing hemangiomas.

Intradural, extramedullary metastases are due to tumor seeding within the leptomeninges and can appear as linear or nodular enhancing lesions along the surfaces of cord or cauda equina nerve roots. Large intradural metastases can also compress the spinal cord (Fig. 2.11a–d). While gadolinium contrast is highly valuable in diagnosing leptomeningeal carcinomatosis, subtle nodular thickening of cauda equina nerve roots can be detected by T2-weighted imaging at high resolution (3 mm or less). If MR imaging is contraindicated, CT myelography can also outline the contours of spinal cord and nerve roots.

Intramedullary metastases are rare although they must be considered in the setting of advanced systemic metastatic disease [71, 72]. These lesions usually demonstrate enhancement and adjacent cord edema (Fig. 2.12a–d), although on imaging they are often not distinguishable from other entities affecting spinal cord, including primary cord neoplasms, inflammatory or infectious pathologies.

Conclusion

Imaging plays a critical role in the diagnosis and management of metastatic disease in the central nervous system. Accurate diagnosis of CNS metastases is an important step in staging. While the imaging appearance of metastases can be highly variable depending on histological subtype of primary tumor, there are a number of important imaging features that can help with diagnosis and treatment planning. The imaging approach to CNS metastasis depends on both clinical symptoms and cancer types in order to maximize the sensitivity of lesion detection.

Acknowledgements This work was supported by the ARRS/ASNR Scholar Award.

References

1. Davis FG, Dolecek TA, McCarthy BJ, Villano JL. Toward determining the lifetime occurrence of metastatic brain tumors estimated from 2007 United States cancer incidence data. Neuro Oncol. 2012;14(9):1171–7.
2. Sloan AE, Nock CJ, Einstein DB. Diagnosis and treatment of melanoma brain metastasis: a literature review. Cancer Control. 2009;16(3):248–55.
3. Delattre JY, Krol G, Thaler HT, Posner JB. Distribution of brain metastases. Arch Neurol. 1988;45(7):741–4.
4. Sze G, Milano E, Johnson C, Heier L. Detection of brain metastases: comparison of contrast-enhanced MR with unenhanced MR and enhanced CT. AJNR Am J Neuroradiol. 1990;11(4):785–91.
5. Gaviani P, Mullins ME, Braga TA, Hedley-Whyte ET, Halpern EF, Schaefer PS, et al. Improved detection of metastatic melanoma by T2*-weighted imaging. AJNR Am J Neuroradiol. 2006;27(3):605–8.
6. Atlas SW, Braffman BH, LoBrutto R, Elder DE, Herlyn D. Human malignant melanomas with varying degrees of melanin content in nude mice: MR imaging, histopathology, and electron paramagnetic resonance. J Comput Assist Tomogr. 1990;14(4):547–54.
7. Enochs WS, Petherick P, Bogdanova A, Mohr U, Weissleder R. Paramagnetic metal scavenging by melanin: MR imaging. Radiology. 1997;204(2):417–23.
8. Hayashi H, Okamoto I, Tanizaki J, Tanaka K, Okuda T, Kato A, et al. Cystic brain metastasis in non–small-cell lung cancer with ALK rearrangement. JCO. 2014;32(36):e122–4.
9. Hwang TL, Valdivieso JG, Yang CH, Wolin MJ. Calcified brain metastasis. Neurosurgery. 1993;32(3):451–454; discussion 454.
10. Tashiro Y, Kondo A, Aoyama I, Nin K, Shimotake K, Tashiro H, et al. Calcified metastatic brain tumor. Neurosurgery. 1990;26(6):1065–70.
11. Deck MD, Messina AV, Sackett JF. Computed tomography in metastatic disease of the brain. Radiology. 1976;119(1):115–20.
12. Yamada N, Imakita S, Sakuma T, Takamiya M. Intracranial calcification on gradient-echo phase image: depiction of diamagnetic susceptibility. Radiology. 1996;198(1):171–8.
13. Collie DA, Brush JP, Lammie GA, Grant R, Kunkler I, Leonard R, et al. Imaging features of leptomeningeal metastases. Clin Radiol. 1999;54(11):765–71.
14. Pirzkall A, McGue C, Saraswathy S, Cha S, Liu R, Vandenberg S, et al. Tumor regrowth between surgery and initiation of adjuvant therapy in patients with newly diagnosed glioblastoma. Neuro Oncol. 2009;11(6):842–52.
15. Hjorthaug K, Højbjerg JA, Knap MM, Tietze A, Haraldsen A, Zacho HD, et al. Accuracy of 18F-FDG PET-CT in triaging lung cancer patients with suspected brain metastases for MRI. Nucl Med Commun. 2015;36(11):1084–90.
16. Colosimo C, Ruscalleda J, Korves M, La Ferla R, Wool C, Pianezzola P, et al. Detection of intracranial metastases: a multicenter, intrapatient comparison of gadobenate dimeglumine-enhanced MRI with routinely used contrast agents at equal dosage. Invest Radiol. 2001;36(2):72–81.
17. Runge VM, Parker JR, Donovan M. Double-blind, efficacy evaluation of gadobenate dimeglumine, a gadolinium chelate with enhanced relaxivity, in malignant lesions of the brain. Invest Radiol. 2002;37(5):269–80.
18. Yuh WT, Tali ET, Nguyen HD, Simonson TM, Mayr NA, Fisher DJ. The effect of contrast dose, imaging time, and lesion size in the MR detection of intracerebral metastasis. AJNR Am J Neuroradiol. 1995;16(2):373–80.
19. Ba-Ssalamah A, Nöbauer-Huhmann IM, Pinker K, Schibany N, Prokesch R, Mehrain S, et al. Effect of contrast dose and field strength in the magnetic resonance detection of brain metastases. Invest Radiol. 2003;38(7):415–22.
20. Nöbauer-Huhmann I-M, Ba-Ssalamah A, Mlynarik V, Barth M, Schöggl A, Heimberger K, et al. Magnetic resonance imaging contrast enhancement of brain tumors at 3 tesla versus 1.5 tesla. Invest Radiol. 2002;37(3):114–9.

21. Hayashida Y, Hirai T, Morishita S, Kitajima M, Murakami R, Korogi Y, et al. Diffusion-weighted imaging of metastatic brain tumors: comparison with histologic type and tumor cellularity. AJNR Am J Neuroradiol. 2006;27(7):1419–25.
22. Duygulu G, Ovali GY, Calli C, Kitis O, Yünten N, Akalin T, et al. Intracerebral metastasis showing restricted diffusion: correlation with histopathologic findings. Eur J Radiol. 2010;74(1):117–20.
23. Haldorsen IS, Espeland A, Larsson E-M. Central nervous system lymphoma: characteristic findings on traditional and advanced imaging. AJNR Am J Neuroradiol. 2011;32(6):984–92.
24. Nemeth AJ, Henson JW, Mullins ME, Gonzalez RG, Schaefer PW. Improved detection of skull metastasis with diffusion-weighted MR imaging. AJNR Am J Neuroradiol. 2007;28(6):1088–92.
25. Chavhan GB, Babyn PS, Thomas B, Shroff MM, Haacke EM. Principles, techniques, and applications of T2*-based MR imaging and its special applications. Radiographics. 2009;29(5): 1433–49.
26. Mittal S, Wu Z, Neelavalli J, Haacke EM. Susceptibility-weighted imaging: technical aspects and clinical applications, part 2. AJNR Am J Neuroradiol. 2009;30(2):232–52.
27. Bruhn H, Frahm J, Gyngell ML, Merboldt KD, Hänicke W, Sauter R, et al. Noninvasive differentiation of tumors with use of localized H-1 MR spectroscopy in vivo: initial experience in patients with cerebral tumors. Radiology. 1989;172(2):541–8.
28. Poptani H, Gupta RK, Roy R, Pandey R, Jain VK, Chhabra DK. Characterization of intracranial mass lesions with in vivo proton MR spectroscopy. AJNR Am J Neuroradiol. 1995;16(8): 1593–603.
29. Sijens PE, Knopp MV, Brunetti A, Wicklow K, Alfano B, Bachert P, et al. 1H MR spectroscopy in patients with metastatic brain tumors: a multicenter study. Magn Reson Med. 1995;33 (6):818–26.
30. Law M. MR spectroscopy of brain tumors. Top Magn Reson Imaging. 2004;15(5):291–313.
31. García-Gómez JM, Luts J, Julià-Sapé M, Krooshof P, Tortajada S, Robledo JV, et al. Multiproject-multicenter evaluation of automatic brain tumor classification by magnetic resonance spectroscopy. MAGMA. 2009;22(1):5–18.
32. Groothuis DR. The blood-brain and blood-tumor barriers: a review of strategies for increasing drug delivery. Neuro-Oncol. 2000; 2(1):45–59.
33. Law M, Cha S, Knopp EA, Johnson G, Arnett J, Litt AW. High-grade gliomas and solitary metastases: differentiation by using perfusion and proton spectroscopic MR imaging. Radiology. 2002;222(3):715–21.
34. Young GS, Setayesh K. Spin-echo echo-planar perfusion MR imaging in the differential diagnosis of solitary enhancing brain lesions: distinguishing solitary metastases from primary glioma. AJNR Am J Neuroradiol. 2009;30(3):575–7.
35. Bertossi M, Virgintino D, Maiorano E, Occhiogrosso M, Roncali L. Ultrastructural and morphometric investigation of human brain capillaries in normal and peritumoral tissues. Ultrastruct Pathol. 1997;21(1):41–9.
36. Cha S. Perfusion MR imaging of brain tumors. Top Magn Reson Imaging. 2004;15(5):279–89.
37. Basser PJ. Inferring microstructural features and the physiological state of tissues from diffusion-weighted images. NMR Biomed. 1995;8(7–8):333–44.
38. Lu S, Ahn D, Johnson G, Cha S. Peritumoral diffusion tensor imaging of high-grade gliomas and metastatic brain tumors. AJNR Am J Neuroradiol. 2003;24(5):937–41.
39. Tsuchiya K, Fujikawa A, Nakajima M, Honya K. Differentiation between solitary brain metastasis and high-grade glioma by diffusion tensor imaging. Br J Radiol. 2005;78(930):533–7.
40. Lu S, Ahn D, Johnson G, Law M, Zagzag D, Grossman RI. Diffusion-tensor MR imaging of intracranial neoplasia and associated peritumoral edema: introduction of the tumor infiltration index. Radiology. 2004;232(1):221–8.
41. Jones TL, Byrnes TJ, Yang G, Howe FA, Bell BA, Barrick TR. Brain tumor classification using the diffusion tensor image segmentation (D-SEG) technique. Neuro-Oncol. 2015;17(3): 466–76.
42. Yang G, Jones TL, Howe FA, Barrick TR. Morphometric model for discrimination between glioblastoma multiforme and solitary metastasis using three-dimensional shape analysis. Magn Reson Med. 2016;75(6):2505–16.
43. Blanchet L, Krooshof PWT, Postma GJ, Idema AJ, Goraj B, Heerschap A, et al. Discrimination between metastasis and glioblastoma multiforme based on morphometric analysis of MR images. AJNR Am J Neuroradiol. 2011;32(1):67–73.
44. Albert FK, Forsting M, Sartor K, Adams HP, Kunze S. Early postoperative magnetic resonance imaging after resection of malignant glioma: objective evaluation of residual tumor and its influence on regrowth and prognosis. Neurosurgery. 1994; 34(1):45–60–61.
45. Forsting M, Albert FK, Kunze S, Adams HP, Zenner D, Sartor K. Extirpation of glioblastomas: MR and CT follow-up of residual tumor and regrowth patterns. AJNR Am J Neuroradiol. 1993;14 (1):77–87.
46. Hartmann M, Jansen O, Heiland S, Sommer C, Münkel K, Sartor K. Restricted diffusion within ring enhancement is not pathognomonic for brain abscess. AJNR Am J Neuroradiol. 2001;22(9):1738–42.
47. Gaensler EH, Dillon WP, Edwards MS, Larson DA, Rosenau W, Wilson CB. Radiation-induced telangiectasia in the brain simulates cryptic vascular malformations at MR imaging. Radiology. 1994;193(3):629–36.
48. Leeman JE, Clump DA, Flickinger JC, Mintz AH, Burton SA, Heron DE. Extent of perilesional edema differentiates radionecrosis from tumor recurrence following stereotactic radiosurgery for brain metastases. Neuro-Oncol. 2013;15(12):1732–8.
49. Zach L, Guez D, Last D, Daniels D, Grober Y, Nissim O, et al. Delayed contrast extravasation MRI: a new paradigm in neuro-oncology. Neuro-Oncol. 2015;17(3):457–65.
50. Larroza A, Moratal D, Paredes-Sánchez A, Soria-Olivas E, Chust ML, Arribas LA, et al. Support vector machine classification of brain metastasis and radiation necrosis based on texture analysis in MRI. J Magn Reson Imaging. 2015;42(5):1362–8.
51. Kang TW, Kim ST, Byun HS, Jeon P, Kim K, Kim H, et al. Morphological and functional MRI, MRS, perfusion and diffusion changes after radiosurgery of brain metastasis. Eur J Radiol. 2009;72(3):370–80.
52. Asao C, Korogi Y, Kitajima M, Hirai T, Baba Y, Makino K, et al. Diffusion-weighted imaging of radiation-induced brain injury for differentiation from tumor recurrence. AJNR Am J Neuroradiol. 2005;26(6):1455–60.
53. Essig M, Waschkies M, Wenz F, Debus J, Hentrich HR, Knopp MV. Assessment of brain metastases with dynamic susceptibility-weighted contrast-enhanced MR imaging: initial results. Radiology. 2003;228(1):193–9.
54. Graves EE, Nelson SJ, Vigneron DB, Verhey L, McDermott M, Larson D, et al. Serial proton MR spectroscopic imaging of recurrent malignant gliomas after gamma knife radiosurgery. AJNR Am J Neuroradiol. 2001;22(4):613–24.
55. Schlemmer HP, Bachert P, Herfarth KK, Zuna I, Debus J, van Kaick G. Proton MR spectroscopic evaluation of suspicious brain lesions after stereotactic radiotherapy. AJNR Am J Neuroradiol. 2001;22(7):1316–24.

56. Griffeth LK, Rich KM, Dehdashti F, Simpson JR, Fusselman MJ, McGuire AH, et al. Brain metastases from non-central nervous system tumors: evaluation with PET. Radiology. 1993;186(1): 37–44.
57. Rohren EM, Provenzale JM, Barboriak DP, Coleman RE. Screening for cerebral metastases with FDG PET in patients undergoing whole-body staging of non-central nervous system malignancy. Radiology. 2003;226(1):181–7.
58. Cicone F, Minniti G, Romano A, Papa A, Scaringi C, Tavanti F, et al. Accuracy of F-DOPA PET and perfusion-MRI for differentiating radionecrotic from progressive brain metastases after radiosurgery. Eur J Nucl Med Mol Imaging. 2015;42(1):103–11.
59. Lin NU, Lee EQ, Aoyama H, Barani IJ, Barboriak DP, Baumert BG, et al. Response assessment criteria for brain metastases: proposal from the RANO group. Lancet Oncol. 2015;16(6):e270–8.
60. Schiff D, O'Neill BP, Suman VJ. Spinal epidural metastasis as the initial manifestation of malignancy: clinical features and diagnostic approach. Neurology. 1997;49(2):452–6.
61. Yu C-W, Hsu C-Y, Shih TT-F, Chen B-B, Fu C-J. Vertebral osteonecrosis: MR imaging findings and related changes on adjacent levels. AJNR Am J Neuroradiol. 2007;28(1):42–7.
62. Baur A, Stäbler A, Arbogast S, Duerr HR, Bartl R, Reiser M. Acute osteoporotic and neoplastic vertebral compression fractures: fluid sign at MR imaging. Radiology. 2002;225(3):730–5.
63. Theodorou DJ. The intravertebral vacuum cleft sign. Radiology. 2001;221(3):787–8.
64. Yuh WT, Zachar CK, Barloon TJ, Sato Y, Sickels WJ, Hawes DR. Vertebral compression fractures: distinction between benign and malignant causes with MR imaging. Radiology. 1989;172(1): 215–8.
65. Cuénod CA, Laredo JD, Chevret S, Hamze B, Naouri JF, Chapaux X, et al. Acute vertebral collapse due to osteoporosis or malignancy: appearance on unenhanced and gadolinium-enhanced MR images. Radiology. 1996;199(2):541–9.
66. Zhou XJ, Leeds NE, McKinnon GC, Kumar AJ. Characterization of benign and metastatic vertebral compression fractures with quantitative diffusion MR imaging. AJNR Am J Neuroradiol. 2002;23(1):165–70.
67. Chan JHM, Peh WCG, Tsui EYK, Chau LF, Cheung KK, Chan KB, et al. Acute vertebral body compression fractures: discrimination between benign and malignant causes using apparent diffusion coefficients. Br J Radiol. 2002;75(891):207–14.
68. Abanoz R, Hakyemez B, Parlak M. Diffusion-weighted imaging of acute vertebral compression: differential diagnosis of benign versus malignant pathologic fractures. Tani Girisim Radyol. 2003;9(2):176–83.
69. Sung JK, Jee W-H, Jung J-Y, Choi M, Lee S-Y, Kim Y-H, et al. Differentiation of acute osteoporotic and malignant compression fractures of the spine: use of additive qualitative and quantitative axial diffusion-weighted MR imaging to conventional MR imaging at 3.0 T. Radiology. 2014;271(2):488–98.
70. Laredo JD, Lakhdari K, Bellaïche L, Hamze B, Janklewicz P, Tubiana JM. Acute vertebral collapse: CT findings in benign and malignant nontraumatic cases. Radiology. 1995;194(1):41–8.
71. Lee SS, Kim MK, Sym SJ, Kim SW, Kim WK, Kim S-B, et al. Intramedullary spinal cord metastases: a single-institution experience. J Neurooncol. 2007;84(1):85–9.
72. Schiff D, O'Neill BP. Intramedullary spinal cord metastases: clinical features and treatment outcome. Neurology. 1996; 47(4):906–12.